Using large-scale diagnostic quantities to investigate change in East Coast Lows

Fei Ji, Jason P. Evans, Daniel Argueso, Lluis Fita & Alejandro Di Luca

Climate Dynamics
Observational, Theoretical and Computational Research on the Climate System

ISSN 0930-7575

Clim Dyn
DOI 10.1007/s00382-015-2481-9

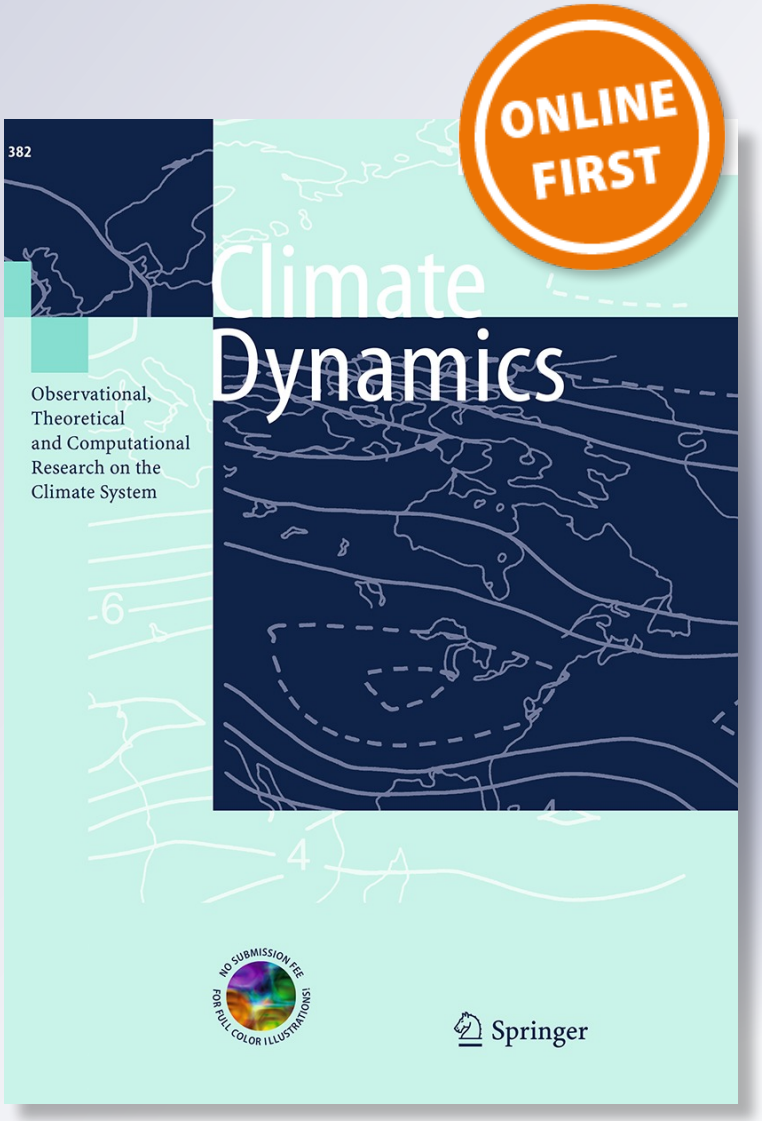

Springer

Clim Dyn
DOI 10.1007/s00382-015-2481-9

Using large-scale diagnostic quantities to investigate change in East Coast Lows

Fei Ji · Jason P. Evans · Daniel Argueso · Lluis Fita · Alejandro Di Luca

Received: 15 June 2014 / Accepted: 12 January 2015

Abstract East Coast Lows (ECLs) are intense low-pressure systems that affect the eastern seaboard of Australia. They have attracted research interest for both their destructive nature and water supplying capability. Estimating the changes in ECLs in the future has a major impact on emergency response as well as water management strategies for the coastal communities on the east coast of Australia. In this study, ECLs were identified using two large-scale diagnostic quantities: isentropic potential vorticity (IPV) and geostrophic vorticity (GV), which were calculated from outputs of historical and future regional climate simulations from the NSW/ACT regional climate modelling (NARCliM) project. The diagnostic results for the historical period were evaluated against a subjective ECL event database. Future simulations using a high emission scenario were examined to estimate changes in frequency, duration, and intensity of ECLs. The use of a relatively high resolution regional climate model makes this the first study to examine future changes in ECLs while resolving the full range of ECL sizes which can be as small as 100–200 km in diameter. The results indicate that it is likely that there will be fewer ECLs, with weaker intensity in the future. There could also be a seasonal shift in ECLs from cool months to warm months. These changes have the potential to significantly impact the water security on the east coast of Australia.

Keywords East Coast Lows (ECLs) · Isentropic potential vorticity (IPV) · Geostrophic vorticity (GV) · NARCliM

1 Introduction

The eastern seaboard of Australia is a different climatological entity to the rest of eastern Australia. Major climate drivers such as the El Nino–Southern Oscillation and the Indian Ocean Dipole have substantially weaker correlations with rainfall in this region than elsewhere in eastern Australia (Murphy and Timbal 2008; Timbal 2010). Recent research suggests that East Coast Lows (ECLs), also known as east coast cyclones, are a dominant driver of climate for the region (Dowdy et al. 2014), that strongly influences extreme rainfall along the eastern seaboard (Imielska et al. 2012; Pepler and Coutts-Smith 2012).

ECLs are intense low-pressure systems that occur, on average, several times each year off the eastern coast of Australia, in particular southern Queensland and New South Wales (NSW). The coastal area is boarded in west by the Great Dividing Range (the most substantial mountain range in Australia) that stretches thousands of kilometres from Queensland, running the entire length of the eastern coastline through NSW, then into Victoria (Fig. 1). ECLs are more common during autumn and winter although they can occur at any time of the year (Hopkin and Holland 1997; Speer et al. 2009). ECLs often intensify rapidly overnight making them one of

F. Ji (✉)
Office of Environment and Heritage, NSW Department of Planning and Environment, 11 Farrer Place, PO. Box 733, Queanbeyan, NSW 2620, Australia
e-mail: fei.ji@environment.nsw.gov.au

J. P. Evans · D. Argueso · L. Fita · A. Di Luca
Climate Change Research Centre and ARC Centre of Excellence for Climate System Science, University of New South Wales, Sydney, NSW, Australia

L. Fita
Laboratoire de Météorologie Dynamique, CNRS, Université Pierre et Marie Curie, Paris, France

Published online: 23 January 2015

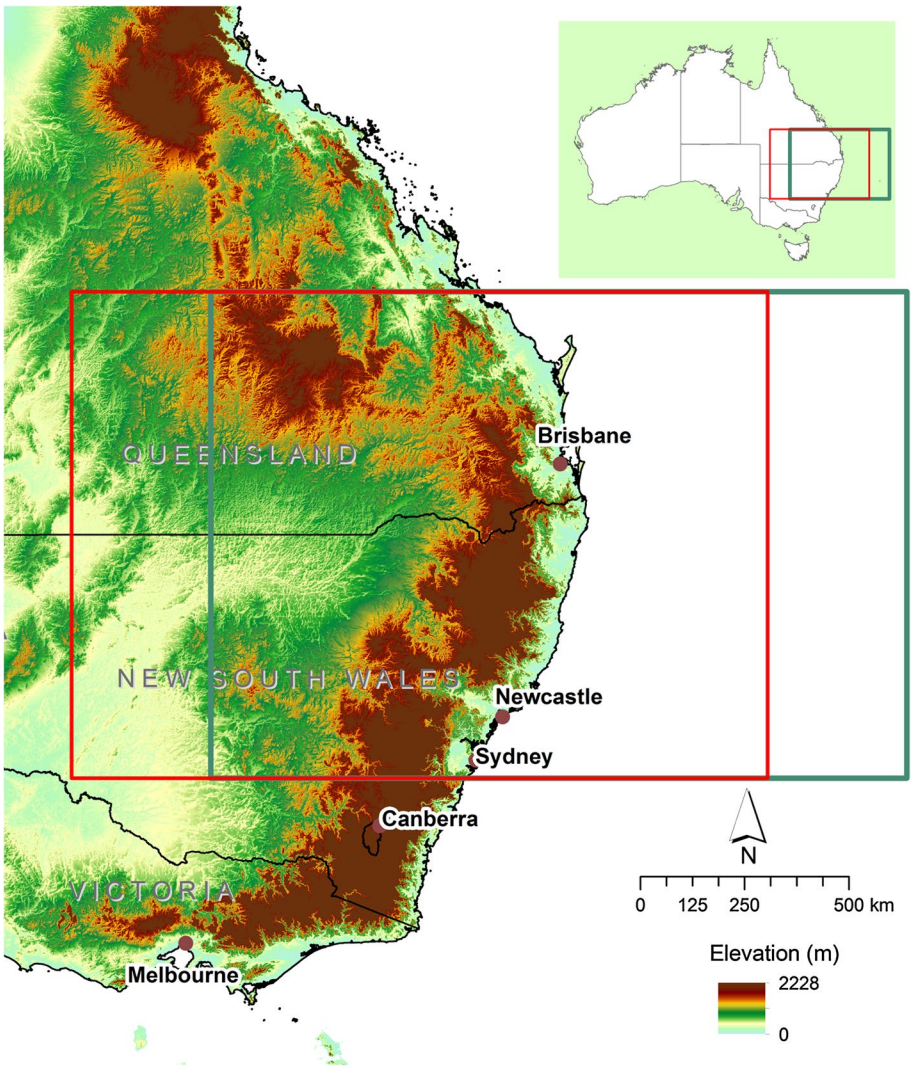

Fig. 1 Map of Australia showing the domains (*red rectangle* and *green rectangle*) used for extracting extreme values of IPV and GV respectively

the more dangerous weather systems to affect the Australian coast. For example, an intense low system on the 8th of June 2007 caused extensive damage along the central NSW coastline near Newcastle (32.93°S, 151.79°E), which is a top 10 natural disaster in Australian history, including nine deaths, major flash flooding, extreme wind gusts and sea waves, over $1.5b in damage (Mills et al. 2010; Verdon-Kidd et al. 2010). Although ECLs can cause significant damage to coastal infrastructure and ecosystems through heavy rainfall and flooding, strong wind gusts, storm waves and increased sea levels, they also contribute positively to the fresh water resources in eastern Australia, particularly in north-eastern NSW (Risbey et al. 2009; Pepler and Rakich 2010). The impact of these ECLs means that any potential trends in their frequency, duration, and intensity have particular importance for both coastal infrastructure planning and also for water resources planning along the eastern seaboard of Australia.

ECLs have mainly been investigated in the context of individual or a group of events (Bridgman 1985; Holland et al. 1987; McInnes et al. 1992; Hopkin and Holland 1997; Leslie and Speer 1998; Qi et al. 2006; Garde et al. 2010; Mills et al. 2010; Verdon-Kidd et al. 2010; Evans et al. 2012; Ji et al. 2011, 2014). There has been some effort to build East Coast Low storm dataset using various classification schemes (PWD 1985, 1986; Holland et al. 1987; Hopkin and Holland 1997; Qi et al. 2006; Speer et al. 2009, 2011). However, most of these classification schemes are subjectively based on surface variables. A recent publication by Browning and Goodwin (2013) uses an objective approach to track ECLs based on the mean sea level pressure. Mills et al. (2010) found that the development of the upper-tropospheric cut-off low over south-east Australia was critical in the explosive surface development of the Pasha Bulker East Coast Low of 8 June 2007. They further analysed 11 of the highest impact ECLs listed by the NSW Regional Forecasting Centre of the Australia

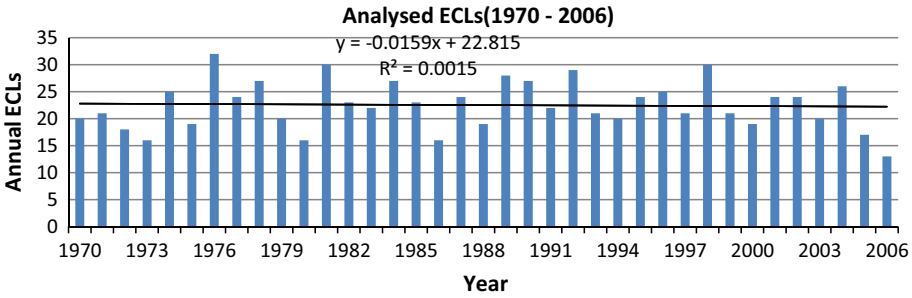

Fig. 2 Annual frequency of ECLs for 1970–2006 in the observational dataset (Speer et al. 2009). The *black line* shows the trend of the annual ECL frequency, equation for the trend line is included

Bureau of Meteorology, finding that they all developed from a large-scale upper-tropospheric cut-off low or large amplitude trough.

Dowdy et al. (2011, 2013a) examined a number of large-scale diagnostic quantities in the upper troposphere associated with ECLs, based on the interim European Centre for Medium-Range Weather Forecasts (ECMWF) Re-Analysis [ERA Interim (ERA-I); Uppala et al. 2005] from 1989 to 2006. Diagnostic quantities based on isentropic potential vorticity (IPV) and geostrophic vorticity (GV) were shown to provide a good indication of the likely occurrence of East Coast Lows, as well as associated impacts such as extreme rainfall events. Dowdy et al. (2013b) further applied the method to two other reanalyses [NNRP (Kalnay et al. 1996) and ERA-40 (Uppala et al. 2005)] and three global climate models (GCMs). The results obtained when applying the diagnostic to two of the three GCMs are similar to expectations given their spatial resolutions, and produce seasonal cycles similar to those from the reanalyses.

This study applies these vorticity based ECL indicators to the finer resolution dynamical downscaling outputs from the NARCliM (New South Wales/Australian Capital Territory regional climate modelling http://www.ccrc.unsw.edu.au/NARCliM/) project (Evans et al. 2014). The multiple model simulations (12 members) allow exploring a large range of variations in the future projections. The finer resolution regional climate model (RCM) simulations are able to resolve smaller atmospheric features than the GCMs. Further, this study explores the seasonal variation of ECLs in greater detail than previous studies (Dowdy et al. 2011, 2013a, b) and investigates changes in duration and intensity of ECLs that have not previously been studied.

The paper is structured as follows; Sect. 2 describes the data used in the study; Sect. 3 describes the methodology for indicating ECL events; Sect. 4 presents the results of changes in frequency, duration, and intensity of ECLs. Discussions and conclusions are presented in Sects. 5 and 6.

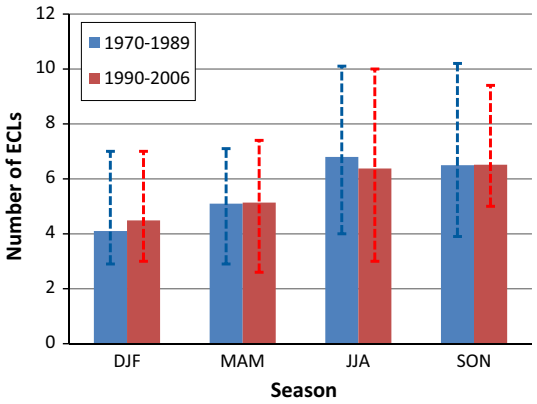

Fig. 3 Observed seasonal frequencies of ECLs for two periods. *Error bars* shows the inter-annual range (10th–90th percentile)

2 Data

2.1 ECL data

The subjectively analysed ECL database (Speer et al. 2009) is the only available "observational dataset" to evaluate objective tracking results. The dataset, that was constructed from daily charts of mean sea level pressure, station data and satellite images, includes details (date, intensity, and category etc.) for each ECL event from 1970 to 2006. Figure 2 shows the number of ECLs per year for this period. For the whole period, there is no obvious trend in annual ECLs. As the observations are limited in length, no obvious trend in this particular period does not necessarily exclude the possibility of ECLs being sensitive to global warming.

We divided the subjective dataset into two time periods (1970–1989 and 1990–2006) to investigate whether there has been any change in the occurrence of ECLs recently. The average numbers of ECLs per year for both periods are almost identical and are about 22.5. When the later period is compared to the earlier period (Fig. 3), the numbers of ECLs in winter (Jun–Aug) have decreased

Table 1 The model configuration for the three RCMs in NARCliM

NARCliM ensemble member	Planetary boundary layer physics/surface layer physics	Cumulus physics	Micro-physics	Shortwave/longwave radiation physics
R1	MYJ/Eta similarity	KF	WDM 5 class	Dudhia/RRTM
R2	MYJ/Eta similarity	BMJ	WDM 5 class	Dudhia/RRTM
R3	YSU/MM5 similarity	KF	WDM 5 class	CAM/CAM

whereas those in summer (Dec–Feb) have increased. We further compared the seasonal distributions between the two equal length periods (1970–1987 and 1988–2005) and results also suggest a seasonal shift in the occurrence of ECLs from cool to warm months, although the shift is not significant, falling well within the range of inter-annual variability.

2.2 NARCliM data

As designed in the NARCliM project, simulations from four GCMs were used to drive three RCMs to form a 12 member GCM/RCM ensemble (Evans et al. 2014). The four selected GCMs are MIROC3.2, ECHAM5, CCCMA3.1, and CSIRO-MK3.0 (Evans and Ji 2012a). For the future projections the SRES A2 emission scenario (IPCC 2000) was used. The three selected RCMs (detailed in Table 1) are three physics scheme combinations of the WRF model (Evans and Ji 2012b). Each simulation consists of three 20-year runs (1990–2009, 2020–2039, and 2060–2079). The model domain covers the Coordinated Regional Climate Downscaling Experiment (CORDEX) (Giorgi et al. 2009) AustralAsia region with 50 km resolution that is much finer than those of the reanalyses data or GCM outputs used in pervious studies (Dowdy et al. 2011, 2013a, b). The fine resolution given by RCMs can provide information that identifies small-sized, weak and short duration low systems that coarse resolution reanalyses data and GCM simulations are incapable of capturing.

Some initial evaluation of NARCliM simulations shows that RCMs have strong skills in simulating the climate of Australia with a small cold bias and overestimation of precipitation on the Great Dividing Range. The differing responses of the different RCMs confirm the utility of considering model independence when choosing the RCMs. The RCM response to large scale modes of variability also reflect the observations well (Evans et al. 2013b). The ability of the models to simulate particular East Coast Lows was examined in Evans et al. (2012), and Ji et al. (2014). Further in-depth evaluations of the ensemble performance for present-day climate are underway. Through these evaluations we find that while there is a spread in model predictions, all models perform adequately with no single model performing the best overall variables and metrics. The use of the full ensemble provides a measure of robustness such that any result that is common through all models in the ensemble is considered to have higher confidence.

We note that the data used in this study are from the NARCliM project in which 4 GCMs and 3 RCMs were chosen based on a number of criteria (Evans et al. 2014): (1) adequate performance when simulating historic climate; (2) most independent; (3) cover the largest range of plausible future climates for Australia (only for selection of GCMs). We acknowledge that the results are model dependent (as all model studies are) but through the use of this carefully selected ensemble we have attempted to minimise this dependence. By using this model selection process we have shown that it is possible to create relatively small ensembles that are able to reproduce the ensemble mean and variance from the parent large ensemble as well as minimise the overall error (Evans et al. 2013a).

For easier description in this paper, the 12 simulations were named MIROC-R1, MIROC-R2, MIROC-R3; ECHAM-R1, ECHAM-R2, ECHAM-R3; CCCMA-R1, CCCMA-R2, CCCMA-R3; and MK30-R1, MK30-R2, MK30-R3. The simulations driven by the same GCM were referred to as GCM simulations, the simulations using the same RCM were referred to as RCM simulations. In total, there were 4 GCM simulations (average of 3 members) and 3 RCMs simulation (average of four members). The analyses in this study are based on the outputs from these 12 simulations.

3 Methodology

3.1 Indicated ECL and ECL frequency

Two diagnostic quantities were calculated based on the NARCliM simulations to objectively investigate changes in ECLs following Dowdy et al. (2011). Isentropic potential vorticity (IPV) was calculated on 320 K isentropic surface.

$$IPV = -g(\xi_\theta + f)\frac{\partial \theta}{\partial p} \quad (1)$$

Here g is gravitational acceleration, ξ_θ is relative vorticity calculated on isentropic surface, f is the Coriolis parameter, $\frac{\partial\theta}{\partial p}$ is lapse rate of potential temperature.

The geostrophic vorticity (GV) was calculated on the 500 hpa pressure level.

$$\xi = \frac{1}{f}\nabla^2\Phi \tag{2}$$

Here f is the Coriolis parameter and $\nabla^2\Phi$ is the Laplacian of geopotential. As vorticity is negative for low pressure systems in the southern hemisphere, GV and IPV were multiplied by -1×10^6 to convert them into (positive) potential vorticity units (PVU $= 10^{-6}$ K m^2/kg/s).

The IPV/GV was calculated at 6 hourly intervals for each of 12 simulations. The extreme maximum values of IPV and GV within the geographic regions of 15° in longitude and 10.5° in latitude centred on 29°S,150°E and 29°S,153°E respectively (see domains in Fig. 1) for each time step were extracted to form an extreme IPV/GV time series (Dowdy et al. 2011, 2013a). Since the observations in Speer et al. (2009) are based on mean sea level pressure rather than vorticity measures, we employed a procedure to establish a relationship between model simulations and observations. A threshold for each month was applied to the extreme IPV/GV time series to objectively identify ECLs. The ECLs identified this way are termed "indicated ECLs" hereafter. In Dowdy et al. (2011, 2013a, b) a single threshold is selected in order to match the mean annual number of ECLs with that identified in the subjective dataset. This results in a poor correspondence between the annual cycles of the two datasets. Here the thresholds were selected so that the average number of ECLs for each month matches that of the observed data for the historical period (1990–2009). Since the observed (subjective) ECL dataset (available from 1970 to 2006) does not cover the entire period of 1990–2009, we assumed that the ECL monthly distribution for 1990–2006 is representative of the period of 1990–2009. The same set of thresholds derived from the historical period was applied to the two future periods to get the indicated future ECLs.

For each of the 12 simulations, the indicated ECLs for the two future periods were compared to the historical period to investigate the changes in annual and monthly ECL frequency.

3.2 IPV/GV indicated ECL duration

The durations for indicated ECLs were calculated based on the number of consecutive occurrences with IPV/GV value above the threshold and averaged to get the mean ECL duration for the three time periods, and for each simulation. The changes in durations were estimated as the differences in mean duration derived from two future periods relative to the historic period.

3.3 IPV/GV indicated ECL intensity

The IPV/GV values above the monthly thresholds were extracted to form a new time series. This new time series was used to analyse ECL intensity. Each time series was sorted from the smallest to largest and divided into bins with width 2 PVU based on the IPV/GV values. The histogram based on the bins above calculated for each of the 36 time series (12 simulations by 3 time periods) were analysed and compared to estimate changes in IPV/GV indicated ECL intensity.

4 Results

4.1 Changes in ECL frequency

4.1.1 Changes in annual ECLs

IPV/GV indicated annual ECLs for three periods derived from the 12 simulations are shown in Fig. 4. As the IPV/GV thresholds were calibrated against the observation, for the historic period, the mean number of ECLs calculated using both diagnostic quantities (IPV/GV) for all simulations is the same as the observations (22.5). Figure 4 also includes an error bar obtained by calculating the 10th and 90th percentile of the time series of annual number of indicated ECLs. All simulations consistently show a decrease in the number of IPV indicated ECLs for the two future periods. The far future decreases are significant at the 95 % level of confidence using a Kolgomorov–Smirnov test in 11 of the 12 projections (except for MIROC-R3). The magnitude of these decreases varies considerably across different simulations, with the largest variation associated with the choice of the driving GCM.

Some simulations display small increases in GV indicated ECL numbers. These include MIROC-R1, MIROC-R2, MIROC-R3, MK30-R1, and MK30-R2. MIROC-R1, MIROC-R2, MK30-R1, and MK30-R2 project slightly more GV indicated ECLs for 2020–2039 but less for 2060–2079. MIROC-R3 projects increase in GV indicated ECLs for both future periods. The magnitude of changes in annual ECLs is much smaller for GV indicated ECLs than IPV indicated ECLs; and for 2020–2039 compared to 2060–2079. Even for GV indicated ECLs the far future decreases are significant at the 95 % level of confidence using a Kolgomorov–Smirnov test in 7 of the 12 projections (ECHAM-R1, ECHAM-R2, ECHAM-R3; CCCMA-R1, CCCMA-R2, CCCMA-R3; and MK30-R1).

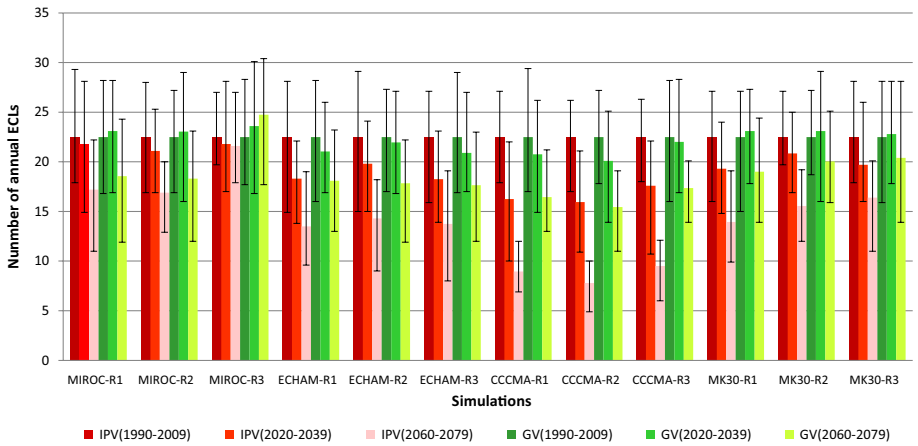

Fig. 4 IPV/GV indicated ECLs for three periods for 12 simulations. The x axis shows 12 simulations, each simulation includes two diagnostic quantities (IPV and GV) and three time periods (1990–2009, 2020–2039 and 2060–2079). *Red columns* shows distributions of IPV indicated ECLs and *green columns* shows distributions of GV indicated ECLs. *Dark*, *medium* and *light colour columns* shows the distribution of indicated ECLs for 1990–2009, 2020–2039 and 2060–2079, respectively. *Error bars* shows the inter-annual range (10th to 90th percentile)

Fig. 5 The same as Fig. 4, but averaged for 4 GCM simulations

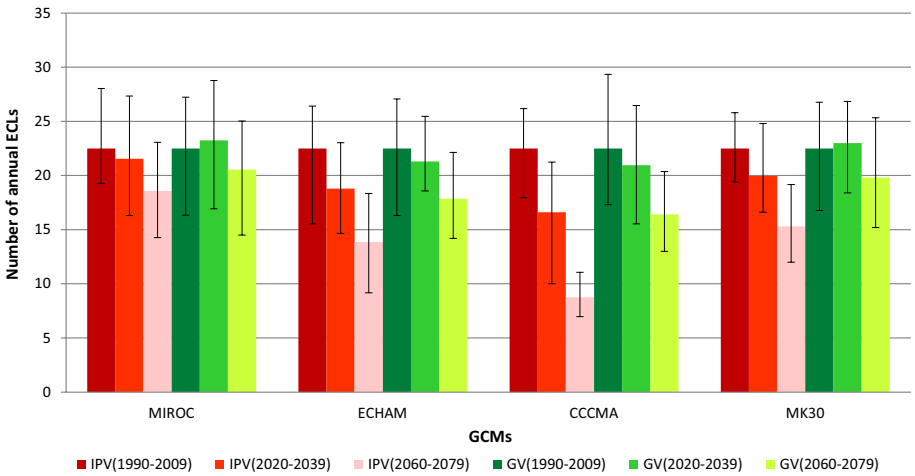

The results for simulations driven by the same GCM were averaged to compare the difference in annual ECLs between the four groups of GCM driven simulations (Fig. 5). All four GCM simulations show decreases or no change in IPV/GV indicated annual ECLs for the future periods. However, the magnitude of decrease differs significantly between the different GCMs. MIROC simulations show smallest decreases, followed by CSIRO-MK3.0 and ECHAM simulations. CCCMA simulations show the largest decrease for both diagnostic quantities, especially for the period of 2060–2079. It is worth noting that the GV indicated ECLs show essentially no change in frequency out to the 2020–2039 period. Both IPV and GV indicated that the rate of changes in annual ECLs is likely to accelerate during this century and the results show good

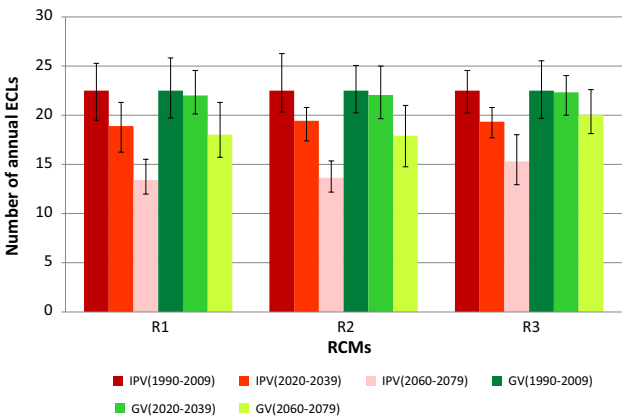

Fig. 6 The same as Fig. 4, but averaged fro 3 RCM simulations

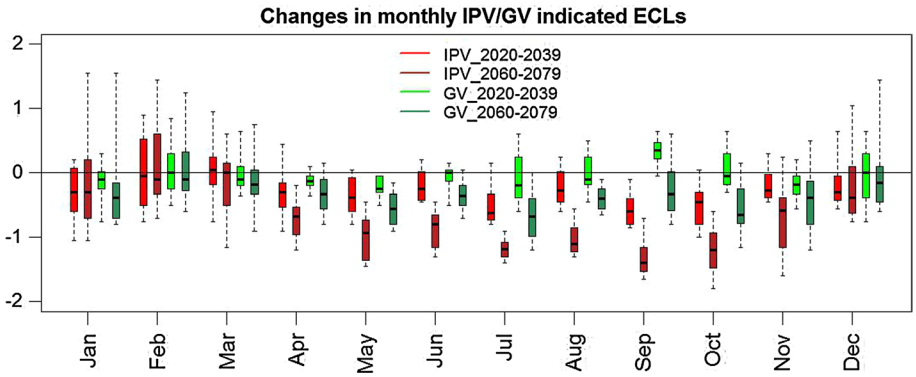

Fig. 7 Plots summarizing changes in monthly IPV/GV indicated ECLs for 12 simulations. The *boxes* and *whiskers* shows the results from 12 simulations. The *boxes* shows the inter-quartile range, the *middle horizontal lines* shows the median and the *whiskers* shows the highest and the lowest values. The results from two diagnostic quantities and two future periods are shown in *different colors*. *Red columns* represent changes in IPV indicated ECLs, *green columns* represent changes in GV indicated ECLs. *Light* and *dark colour columns* shows the changes for 2020–2039 and 2060–2079 relative to 1990–2009, respectively

consistency between different GCM siumulations and RCM simulations (see also Fig. 6).

The results for simulations using the same RCMs were averaged to compare the difference in annual ECLs (Fig. 6). Again, all three RCM simulations show a decreasing trend in IPV/GV indicated annual ECLs for the future periods. The differences between RCM simulations are much smaller than those between GCM simulations, for both GV and IPV indicated ECLs. The magnitude of decrease in annual ECLs is slightly smaller for R3 simulation, following by R2 simulations and R1 simulations. It is worth noting that the IPV indicated far future (2060–2079) changes fall outside the range of inter-annual variaibility.

Taking the overall mean change from the 12 simulations we can obtain quantitative estimates for the 2020–2039 and 2060–2079 periods. There are 0.4 and 3.8 fewer GV indicated ECLs annually for the two future periods respectively; and 3.3 and 8.4 fewer IPV indicated ECLs for the two future periods respectively.

4.1.2 Changes in monthly ECLs

The average number of IPV/GV indicated ECLs for each of the 12 months derived from the 12 simulations were used to investigate the changes in monthly IPV/GV indicated ECLs for future periods relative to the historical period (Fig. 7). There are large differences between the simulations, but most of the simulations show a decreasing trend in the cool months and little change or an increasing trend in the warm months for both of the future periods.

In Fig. 7 it can be seen that there is strong agreement across all simulations for a decrease in IPV indicated ECLs from April through October, by 2060–2079. A fairly consistent decrease of one IPV indicated ECL per month in the cool season is projected. This decrease is significant in at least 8 of the projections (MIROC-R1, MIROC-R2; ECHAM-R1, ECHAM5-R2, ECHAM-R3; and CCCMA-R1, CCCMA-R2, CCCMA-R3) from May to October (excluding June) according to a Kolgomorov–Smirnov test at the 95 % level of confidence. Negative changes projected for the near future using IPV are also quite consistent across simulations for the cool season. In most cases the 25th percentile change is below zero, which means that at least 9 out of 12 simulations project a decrease for IPV indicated ECLs.

In terms of GV indicated ECLs, few changes are consistent across all models. The change in May, July, and August, between present day and far future (2060–2079), are the only months in which all models agree that there will be a decrease in GV indicated ECLs. During cold season months the majority of models also agree with this decrease in ECLs in the far future, though few of these decreases are significant. The mean cold season decrease estimated using GV indicated ECLs is around half of the decrease estimated using IPV indicated ECLs. For the near future there is little consistency in the changes estimated by the 12 models.

4.2 Changes in ECL duration

The mean duration of IPV/GV indicated ECLs are shown in Fig. 8. 11 in 12 simulations showed consistent decreases in IPV indicated ECL duration for both future periods, with the largest decreases in the CCCMA driven simulations, and the smallest far-future decrease in the CSIRO-MK3.0 driven simulations (Fig. 8). For GV indicated ECL durations, only 9 out of 12 simulations showed a decreasing trend with the largest decrease in the CCCMA driven simulations as well. MIROC-R3, ECHAM-R1, and ECHAM-R3 showed increases in GV indicated ECL duration. Most

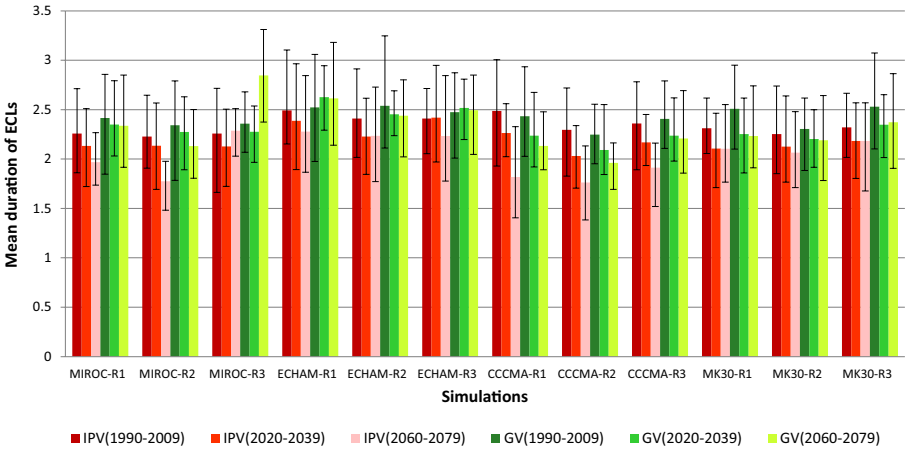

Fig. 8 Mean duration of *IPV/GV* indicated ECLs for 12 simulations The legend is the same that in Fig. 4

of the increases were small except MIROC-R3 simulation for 2060–2079. In general the future duration of ECLs falls within the current inter-annual variability. For IPV indicated ECLs, 4 of 12 models (MIROC-R2, CCCMA-R1, CCCMA-R2 and CCCMA-R3) simulate far future durations outside this range, indicating significant decreases in duration. For GV indicated ECLs, 1 of 12 models (CCCMA-R2) simulates a change outside this range indicating a significant decrease in duration for that particular model only.

The IPV/GV indicated ECL durations for 12 simulations were averaged to calculate the most likely change in duration. Both diagnostic quantities showed decreases in mean duration, while a larger reduction in duration was projected for IPV indicated ECLs compared to GV indicated ECLs. The duration was projected to be ~2.5 h shorter for GV indicated ECLs for both future periods, and 3.5 h shorter for IPV indicated ECLs for 2020–2039, and 7 h shorter for IPV indicated ECLs for 2060–2079. It should be noted that these mean changes in duration have limited confidence as they fall within the range of interannual variability.

4.3 Changes in ECL intensity

All simulations projected decreased intensity for IPV indicated ECLs. Most of the simulations (11 out of 12) also projected decrease/no change in intensity for GV indicated ECLs. MIROC-R3 simulation, being an exception, projected an increase in GV indicated ECL intensity, as well as an increase in annual ECL numbers and mean duration as shown in Sects. 4.1 and 4.2.

The 3 RCM simulations generally showed similar results with the R1 simulation giving slightly larger decreases than R2 and R3 driven simulations. There are clear differences in the results given by the 4 GCM simulations with the CCCMA simulation projecting the largest decrease, followed by ECHAM, CSIRO-MK3.0, and MIROC simulations.

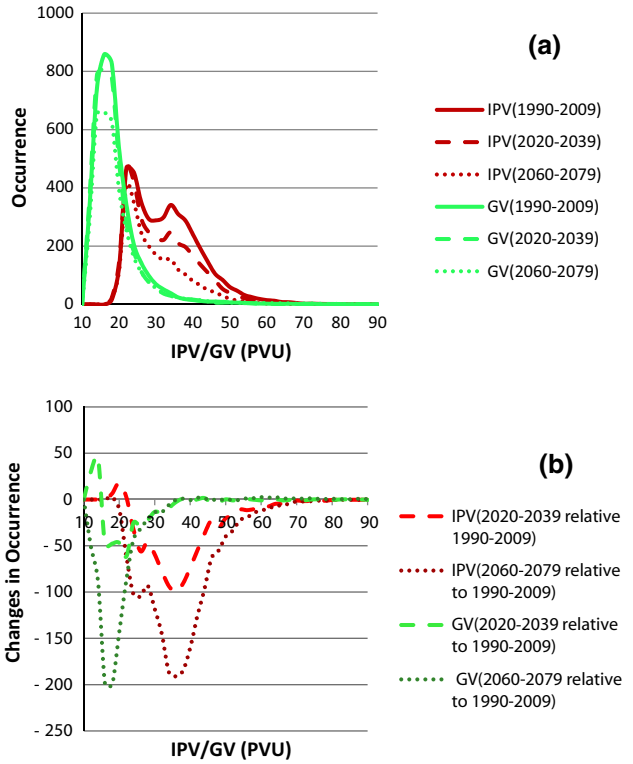

Fig. 9 Mean estimation of IPV/GV occurrence distributions for three time periods (**a**) and their changes for two future periods relative to the historical period (**b**)

Figure 9a shows the distribution of IPV/GV values as number of times (above threshold) in each of the 42 bins at 2 PVU intervals ranging from 10 to 90 PVU. The GV distributions for the three time periods were similar, with a singular peak centred at around 15 PVU. The IPV distributions for the three time periods had dual peaks centred at around 22 and 34 PVU. The most likely change (average of the 12 simulations) in IPV/GV distribution for the two future periods is shown in Fig. 9b. There was a decrease in GV distribution mostly near the peak values

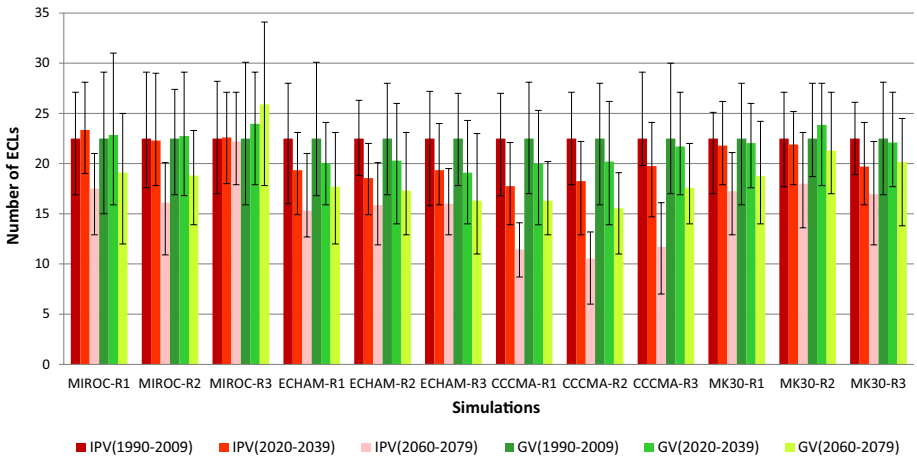

Fig. 10 Annual *IPV/GV* indicated ECLs for 12 simulations using annual thresholds. The legend is the same as that in Fig. 4

for the two future periods. The changes in IPV distribution were mostly near the second peak at 34 PVU. Relatively little change can be observed at the first peak in the IPV distribution. The magnitude of decrease in IPV/GV distributions was larger for 2060–2079 than 2020–2039, relative to 1990–2009. In both cases there is a decrease in the numbers of ECLs with mid-range intensity, while the occurrence of the weakest and the strongest ECLs remains largely unchanged.

5 Discussion

5.1 Impact of choosing different thresholds

In this study, we used a different threshold for each month to identify ECLs. The thresholds were selected so that the average number of ECLs for each month matches that of the observed data for the historic period. Previous studies that used the same threshold for every month (Dowdy et al. 2011, 2013a, b) result in a different initial monthly ECL distribution. It is worth asking whether the changes in the future are sensitive to this difference in the initial distribution. To investigate this, we used the same threshold for each month, referred to as "annual threshold", and compared the results to those from using a different threshold for each month, referred to as "monthly threshold". The annual threshold was determined so that the total ECLs per year for the historic period matched the observations (22.5). Figure 10 shows the IPV/GV indicated ECLs for the 12 simulations using annual threshold. When compared with Fig. 4, which is the same result derived using monthly thresholds, the similarity is evident. There are only small differences in the magnitude of the changes. The same comparison was made for changes in monthly ECL distribution with similar results. This suggests that, choosing either monthly or annual thresholds has little impact on the changes in the future, although the ECL monthly distributions are quite different.

5.2 Impact of choosing different diagnostic quantities

The results in this study showed that the magnitude of changes in IPV indicated ECLs were much larger than those in GV indicated ECLs. This is, at least partially, related to the two diagnostic quantities being calculated on different surfaces. GV was calculated at 500 hpa pressure level, whereas IPV was calculated at 320 K Isentropic level, which is generally more curved (relative to the ground surface). The two diagnostic quantities generally showed the same direction of change in annual and monthly ECLs, intensity and duration. The agreement between the two diagnostic quantities gives us more confidence in the projected trend. However, future warming at the surface will have a direct impact on the height of the 320 Isentropic level and 500 hpa pressure surface and this change in height is responsible for some of the changes seen in the IPV and GV indicated ECLs. The height of 500 hpa surface in the future is higher than its present height however the height of 320 K Isentropic surface is lower than its present height. If this change in height is taken into account (IPV/GV for future periods is calculated at a similar height of isentropic level/pressure level for the present period), the magnitude of changes in GV indicated ECLs increases by 10–20 %, while for IPV indicated ECLs the changes decrease by 30–40 %. This brings the estimated decrease in number of future ECLs into better agreement between GV and IPV indicated ECLs, though IPV still suggests a larger decrease. These changes apply consistently to the decrease seen in colder months, while warm months see no changes or possibly an increase in ECL numbers. As the number of IPV indicated ECLs is more sensitive to this change in height, the GV indicated ECL results could be considered more robust.

5.3 Impact of choosing different GCMs and RCMs

Unlike the three RCMs, which were selected from 36 physics scheme combinations of the WRF model (Skamarock et al. 2008) based on a performance and independence test, the four GCMs selected in the NARCliM project were chosen based on a number of criteria (as described in Sect. 2.2). MIROC3.2 projects a slightly warmer and much wetter future, CCCMA3.1 extremely warmer and slightly wetter, CSIRO-MK3.0 slightly warmer and drier, and ECHAM5 projected an extremely warmer and slightly drier future. Therefore it is not surprising to see that in most of the results, the differences between the GCM simulations are much larger than the differences between the RCMs. This is consistent with the findings from the previous uncertainty studies, which suggests that the largest uncertainty in future projections is sourced from GCM simulations (Chen et al. 2011; Teng et al. 2012). The warmer the GCM projected future climate, the larger are the changes in height of 320 K isentropic and 500 hpa surface level. As discussed in Sect. 5.2 this impacts the projected changes in ECLs and explains at least some of the differences between the GCM projections.

6 Conclusion

In this study, two large scale diagnostic quantities (IPV and GV) were calculated from the NARCliM outputs and were used to investigate the changes in ECLs for two future time periods (2020–2039 and 2060–2079) relative to a historic period (1990–2009). For the reason that the diagnostic threshold is both model and resolution dependent (Dowdy et al. 2013b), the IPV/GV thresholds were selected so that the average number of ECLs for each month matches that of the observed data for the historical period (1990–2009). The same sets of thresholds were used to investigate not only changes in indicated annual ECLs but also changes in monthly distribution, mean duration and intensity of indicated ECLs.

All 12 simulations consistently showed a decreasing trend in frequency for IPV indicated annual ECLs for the two future periods. 7 out of 12 and 11 out of 12 simulations showed the same decreasing trend in frequency for GV indicated ECLs for 2020–2039 and 2060–2079 respectively. This decrease in frequency of IPV indicated and GV indicated events is ~36 and 16 % respectively. This compares well with the ~30 % decrease in the frequency of events estimated by GCMs driven by a high emission scenario reported in Dowdy et al. (2013b).

The majority of simulations projected reduced IPV indicated monthly frequency of ECLs in cool months and little change in warm months. Most simulations also projected similar changes in GV indicated ECLs, especially for the period of 2060–2079. These results indicated a possible seasonal shift in the proportion of IPV/GV indicated ECLs from cool to warm months.

The majority of simulations showed shortened durations for IPV indicated ECLs, and most simulations demonstrated the same trend of decrease in duration for GV indicated ECLs. CCCMA simulation show the largest decrease in mean duration, and R1 and R2 simulations show larger decrease in mean duration than R3 simulation, for both IPV/GV indicated ECLs. MIROC-R3 was the only simulation that projected not only strong increases in ECL durations but also increases in annual ECLs and intensity for GV indicated ECLs. The projected changes in duration contain more uncertainty than those for ECL frequency as most duration changes fall within the inter-annual variability.

The differences between GCM simulations were much larger than those between RCM simulations. Four GCM simulations projected substantially different magnitude of changes. Three RCM simulations generally projected similar results in terms of changes in ECLs. Hence the major uncertainties in projected changes in ECLs were from using different GCMs.

The magnitude of changes in ECLs was larger for 2060–2079 than 2020–2039. This indicated that the rate of changes in ECLs is likely to accelerate during this century. For 2060–2079, more simulations showed agreement in the projection of a decrease in annual number, decrease in monthly ECL in cool months and relatively unchanged in warm months, and decrease in duration and intensity.

The magnitude of changes in ECLs was larger for IPV indicated ECLs than GV indicated ECLs, even though the two diagnostic quantities generally provided similar change direction for most of simulations. Due to the strong sensitivity to the change in height of the 320 K isentropic surface in the future, the GV changes are considered a more robust indicator of likely future change than the IPV changes.

In summary, the results for this study indicated that the total number of annual ECLs is likely to decrease in the future, there may be a shift in the proportion of ECLs from cool to warm months, and ECLs defined by these diagnostic quantities may become weaker and shorter in duration. These changes in ECLs could significantly impact water security on the east coast of Australia as ECLs are major contributors to coastal reservoir inflows.

Acknowledgments This work is made possible by funding from the NSW Environmental Trust for the ESCCI-ECL project, the NSW Office of Environment and Heritage backed NSW/ACT Regional Climate Modelling Project (NARCliM), and the Australian Research Council as part of the Future Fellowship FT110100576 and Linkage Project LP120200777. We thank Acacia Pepler and Andrew Dowdy for providing subjective analysed ECL data and useful discussions. The modelling work was undertaken on the NCI high performance computers in Canberra, Australia, which is supported by the Australian Commonwealth Government.

References

Bridgman H (1985) The Sygna storm at Newcastle—12 years later. Meteorol Aust, VBP 4574, 10–16

Browning S, Goodwin I (2013) Large scale influences on the evolution of winter subtropical maritime cyclones affecting Australia's east coast. Mon Weather Rev. doi:10.1175/MWR-D-12-00312.1

Chen J, Brissette FP, Poulin A, Leconte R (2011) Overall uncertainty study of the hydrological impacts of climate change for a Canadian watershed. Water Resour Res 47:W12509

Dowdy AJ, Mills GA, Timbal B (2011) Large-scale indicators of Australian East Coast Lows and associated extreme weather events. CAWCR technical report 37

Dowdy AJ, Mills GA, Timbal B (2013a) Large-scale diagnostics of extratropical cyclogenesis in eastern Australia. Int J Climatol 33(10):2318–2327. doi:10.1002/joc.3599

Dowdy AJ, Mills GA, Timbal B, Wang Y (2013b) Changes in the risk of extratropical cyclones in eastern Australia. J Clim 26(4):1403–1417. doi:10.1175/JCLI-D-12-00192.1

Dowdy AJ, Mills GA, Timbal B, Wang Y (2014) Fewer large waves for eastern Australia due to decreasing storminess. Nature Climate Change. doi:10.1038/NCLIMATE2142

Evans JP, Ji F (2012a) Choosing GCMs. NARCliM technical note 1, NARCliM Consortium, Sydney, Australia, 7 pp

Evans JP, Ji F (2012b) Choosing the RCMs to perform the downscaling. NARCliM technical note 2, NARCliM Consortium, Sydney, Australia, 8 pp

Evans JP, Ekstrom M, Ji F (2012) Evaluating the performance of a WRF physics ensemble over South-East Australia. Clim Dyn 39:1241–1258. doi:10.1007/s00382-011-1244-5

Evans JP, Ji F, Abramowitz G, Ekstrom M (2013a) Optimally choosing small ensemble members to produce robust climate simulations. Environ Res Lett 8:044050. doi:10.1088/1748-9326/8/4/044050

Evans JP, Fita L, Argüeso D, Liu Y (2013b) Initial NARCliM evaluation. In Piantadosi J, Anderssen RS, Boland J (eds) MODSIM2013, 20th international congress on modelling and simulation. Modelling and Simulation Society of Australia and New Zealand, December 2013, pp 2765–2771. ISBN: 978-0-9872143-3-1

Evans JP, Ji F, Lee C, Smith P, Argüeso D, Fita L (2014) Design of a regional climate modelling projection ensemble experiment—NARCliM. Geosci Model Dev 7(2):621–629. doi:10.5194/gmd-7-621-2014

Garde LA, Pezza AB, Tristram Bye JA (2010) Tropical transition of the 2001 Australian Duck. Mon Weather Rev 138:2038–2057. doi:10.1175/2009MWR3220.1.

Giorgi F, Jones C, Asrar GR (2009) Addressing climate information needs at the regional level: the CORDEX framework. WMO Bull 58:175–183

Holland GJ, Lynch AH, Leslie LM (1987) Australian east-coast cyclones. Part I: synoptic overview and case study. J Clim 115:3024–3036

Hopkin LC, Holland GJ (1997) Australian heavy-rain days and associated east coast cyclones: 1958–92. J Clim 10:621–635. doi:10.1175/1520-0442(1997)010<0621:AHRDAA>2.0.CO;2

Imielska A, Alexander L, Timbal B (2012) Extreme rainfall variability on the eastern Seaboard of Australia. In: AMOS annual conference 2012 abstract book, p 145

IPCC (2000) IPCC special report on emission scenarios. In: Nakicenovic N, Swart R. Cambridge University Press, UK

Ji F, Evans JP, Ekstrom M (2011) Using dynamical downscaling to simulation rainfall for East Coast Low events. In: Chan F, Marinova D, Anderssen RS (eds) MODSIM2011, 19th international congress on modelling and simulation. Modelling and Simulation Society of Australia and New Zealand, December 2011, pp 1652–1658. ISBN: 978-0-9872143-1-7. www.mssanz.org.au/modsim2011/F5/ji.pdf

Ji F, Ekstrom M, Evans JP, Teng J (2014) Evaluating rainfall patterns using physics scheme ensembles from a regional atmospheric model. Theoret Appl Climatol 115:297–304. doi:10.1007/s00704-013-0904-2

Kalnay E et al (1996) The NCEP/NCAR 40-year reanalysis project. Bull Am Meteorol Soc 77:437–471

Leslie LM, Speer MS (1998) Short-range ensemble forecasting of explosive Australian east coast cyclogenesis. Weather Forecast 13(3):822–832. doi:10.1175/1520-0434(1998)013<0822:SREFOE>2.0.CO;2

McInnes K, Leslie L, McBride J (1992) Numerical simulation of cut-off lows on the Australian east coast: sensitivity to sea-surface temperature. Int J Climatol 12:783–795

Mills GA, Webb R, Davidson N, Kepert J, Seed A, Abbs D (2010) The Pasha Bulker east coast low of 8 June 2007. CAWCR technical report no. 23. Centre for Australian Weather & Climate Research, Melbourne, Australia

Murphy B, Timbal B (2008) A review of recent climate variability and climate change in south-eastern Australia. Int J Clim 28:859–879. doi:10.1002/joc.1627

Pepler AS, Rakich CS (2010) Extreme inflow events and synoptic forcing in Sydney catchments. IOP Conf Ser: Earth Environ Sci 11:012010. doi:10.1088/1755-1315/11/1/012010

Pepler AS, Coutts-Smith A (2012) Climatological influences on rainfall on the Easteran Seaboard of Australia, and the impact of East Coast Lows, AMOS annual conference 2012 abstract book, p 143

PWD (1985) Elevated coastal levels; storms affecting N.S.W. coast 1880–1980. Report prepared by Blain, Bremner & Williams Pty Ltd in conjunction with Weatherex Meteorological Services Pty Ltd. Public Works Department. Report no 85041

PWD (1986) Elevated coastal levels; storms affecting N.S.W. coast 1980–1985. Report prepared by Lawson and Treloar Pty Ltd in conjunction with Weatherex Meteorological Services Pty Ltd. Report no 8602

Qi L, Leslie L, Speer M (2006) Climatology of cyclones over the southwest Pacific: 1992–2001. Meteorol Atmos Phys 91:201–209. doi:10.1007/s00703-005-0149-4

Risbey JS, Pook MJ, McIntosh PC, Wheeler MC, Hendon HH (2009) On the remote drivers of rainfall variability in Australia. Mon Weather Rev 137:3233–3253. doi:10.1175/2009MWR2861.1

Skamarock WC, Klemp JB, Dudhia J, Gill DO, Barker DM, Duda M, Huang XY, Wang W, Powers JG (2008) A Description of the advanced research WRF version 3. NCAR technical note, NCAR, Boulder, CO, USA

Speer MS, Wiles P, Pepler A (2009) Low pressure systems off the New South Wales coast and associated hazardous weather: establishment of a database. Aust Meteorol Oceanogr J 58:29–39

Speer MS, Leslie LM, Fierro AO (2011) Australian east coast rainfall decline related to large scale climate drivers. Clim Dyn 36:1419–1429. doi:10.1007/s00382-009-0726-1

Teng J, Vaze J, Chiew FHS, Wang B, Perraud J-M (2012) Estimating the relative uncertainties sourced from GCMs and hydrological models in modeling climate change impact on runoff. J Hydrometeorol 13(1):122–139

Timbal B (2010) The climate of the eastern seaboard of Australia: a challenging entity now and for future projections. In: IOP conference series: earth and environmental science, vol 11, p 012013

Uppala SP et al (2005) The ERA-40 re-analysis. Q J R Meteorol Soc 131:2961–3012. doi:10.1256/qj.04.176

Verdon-Kidd DC, Kiem AS, Willgoose G, Haines P (2010) East Coast Lows and the Newcastle/Central Coast Pasha Bulker storm. Report for the National Climate Change Adaptation Research Facility, Gold Coast, Australia